Effect of Solidification Rate on Solidification Structure in Weld Metal†

Yoshiaki ARATA*, Fukuhisa MATSUDA** and Kazuhiro NAKATA***

Abstract

Effects of solidification rate on solidification structure were investigated using moving heat sources of welding arc and electron beam. Solidification rate was varied in the wide range from about 10 to 10^7°C/sec by means of variation of welding heat input for AISI310 austenitic stainless steel and Fe-20 (wt%) Mn alloy.

The sizes in the columnar grains and the primary and the secondary arm spacings in the subgrains were measured in the inward location in the weld metal. Moreover the relations between the arm spacings and the solidification rate in weld metal were investigated.

1. Introduction

The solidification structures in the solidified metal are greatly influenced with the variation of the solidification rate in general. In the field of casting, therefore, which is relatively a slow solidification rate and easy to measure the temperature distribution during solidification, there are many reports, so far, for the relations between the feature in the solidification structure and the solidification variables. In the field of welding, however, there is no systematic report within authors' knowledge except the report for aluminum weld solidification by Brown et al[1]. The solidification of the weld metal is usually a typical rapid solidification. Moreover the solidification rate of the molten metal during welding can be extremely raised to about 10^6 to 10^7 °C/sec with the adoption of electron beam process of high power density and high speed welding.

Therefore the authors have treated in this report the features in the solidification structure of the weld metals which were solidified in the wide range rates with the use of TIG arc and electron beam moving heat sources.

As the features in the solidification structure of the weld metal, the variations of the columnar crystal grain size and the primary and the secondary arm spacings in the subgrains were observed in the weld metals of AISI 310 stainless steel and Fe-20 (wt%) Mn binary alloy which were solidified for various solidification rates.

2. Experimental Procedure

2.1 Materials used

Materials used in this experiment are AISI 310 fully austenitic stainless steel of 9 mm thick plate and Fe-20 (wt%) Mn binary alloy of 14 mm thick plate whose compositions after vacuum melting is 20.1 (wt%) Mn in commercially pure Iron. There are no phase change during and just after solidification.

2.2 Welding Conditions and Observations of Weld Metal Structure

Bead-on-plate welding was done for making all the weld metal using TIG arc (dcsp) and electron beam in vacuum less than 10^{-4} Torr. The welding variables are tablated in Table 1. The cooling rate during solidification was varied with the variation of welding current and welding speed.

Table 1 Welding Conditions used in this experiment.

	Welding voltage	Welding current	Welding speed
TIG Arc	15–21V	150–350A	10 cm/min
EBW	150kV	0.2–30 mA	20–4000 cm/min

The solidification structure of the weld metal was observed at the weld surface after mechanical polish and chemical etching of aqua regia for 310 stainless steel and

† Received on Jan.10, 1976
* Professor
** Associate Professor
*** Graduate Student

5% nitric solution for Fe-20% Mn alloy. In the measurement of the size in columnar crystal grains and subgrains, the grains of which grew vertical direction to the weld ripple line were selected in the weld metal and were measured on an average in the transverse direction.

2.3 Estimation of Solidification Rate

The dimension of the molten puddle during welding is very small and also the cooling rate is so fast that the actual cooling rate is difficult to measure in general. This is particular in the case of low weld heat input. Therefore in this report the cooling rate along the center line of the weld metal was estimated with the use of the equations for the ideal moving heat source[2].

For a three dimensional point heat source

$$\text{Cooling Rate (at } T = T_m) = 2\pi\lambda\cdot(V/Q)\cdot(T_m - T_o)^2 \quad (1)$$

For a two dimensional line heat source

$$\text{Cooling Rate (at } T = T_m) = 2\pi\lambda\cdot C\cdot\rho\cdot(V\cdot h/Q)^2\cdot(T_m - T_o)^3 \quad (2)$$

where, λ: thermal conductivity of metal, C: specific heat, ρ: density, h: thickness of metal, Tm: melting temperature, To: initial temperature, V: welding speed, Q: heat input for welding ($= 0.24\cdot\eta E\cdot I$), η: thermal efficiency to metal, E: arc voltage for TIG and accelerating voltage for electron beam, I: welding current.

The adoption of the equation (1) or (2) to the weld bead was decided after the calculation of the critical thickness, h_c, for the given welding variables, which is given by[3]

$$h_c = [\{1/C\cdot\rho\cdot(T_m - T_o)\}\cdot(Q/V)]^{1/2} \quad (3)$$

Then, the equation (1) is used in case of $h_c < h$, and (2) for $h_c > h$.

In this report the following values were selected as physical constant, that is, λ: 0.055 (cal/cm sec°C) (for AISI 310) and 0.043 (for Fe-20%Mn), C: 0.14 and 0.11 (cal/g °C), ρ: 7.90 and 7.78 (g/cm^3), T_m: 1430 and 1456 (°C), respectively, T_o: 20 (°C), and η: 0.6 for TIG arc and 0.8 for electron beam weldings.

The difference between the calculated cooling rates with the equation (1) and (2) and the measured those with a W-W·26 Re thermocouples was investigated for TIG arc weld metals in the range of relatively low cooling rate using the data in the previous reports[4-6] and by the authors. The result is shown in Fig. 1. In higher solidification rate in the figure the actual cooling rates measured show lower value than the calculated but the difference between them is not so serious in general. Therefore the authors have adopted the calculated value as the solidification rate of the weld center in this report.

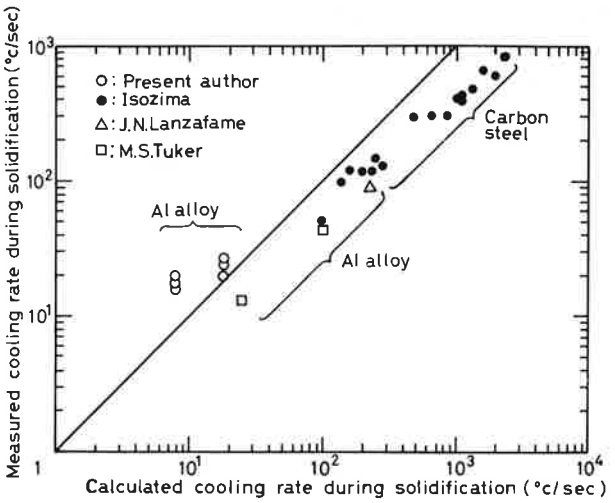

Fig. 1 Comparison of Measured Cooling Rate with Calculated Cooling Rate during Weld Solidification.

3. Experimental Results

3.1 Size of Columnar Crystal Grain in Weld Metal

The relation between the mean width of the columnar crystal grains (W) at the fusion boundary and the weld heat input (E·I/V) is shown for AISI 310 austenitic stainless steel in Fig. 2.

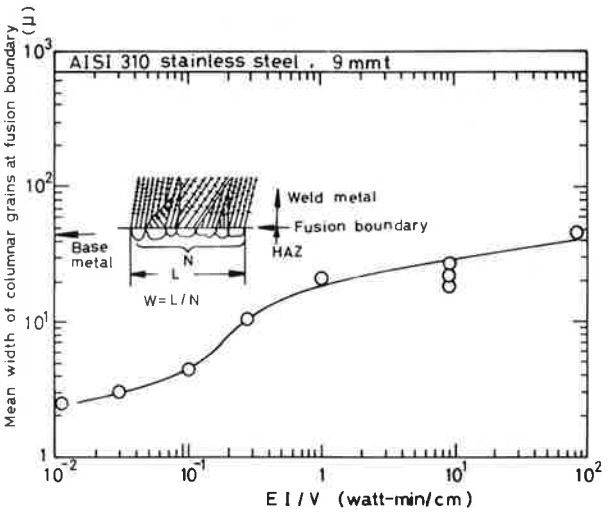

Fig. 2 Variation of Mean Width of Columnar Grains at Fusion Boundary with Welding Heat Input (E·I/V).

The mean width of the grains shows a great increase with the increasing of the weld heat input up to about 1 watt·min/cm and subsequently little increase.

The width of the columnar grains which were

welded in lower weld heat input is narrower than the mean grain size (about 45μm) of the base as indicated in the figure. The reason is considered that the grains in the HAZ were getting finer due to the recrystallization with a rapid thermal heating.

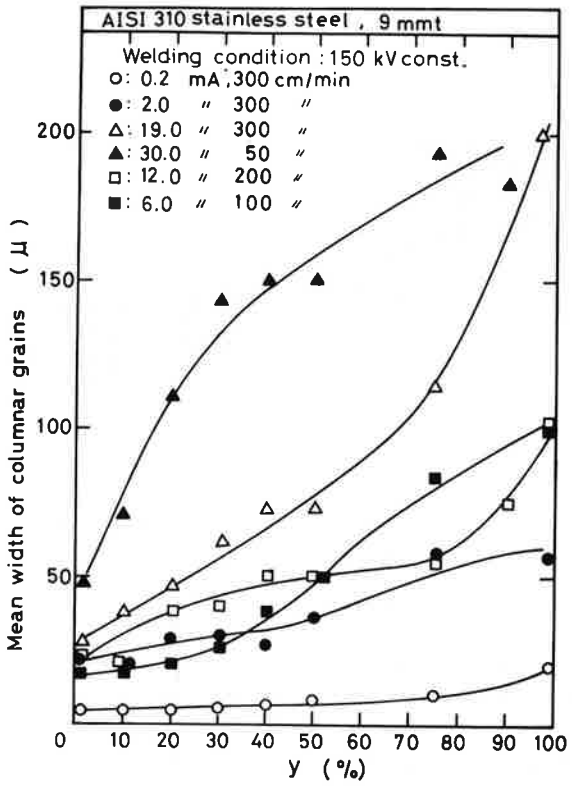

Fig. 3 Variation of Mean Width of Columnar Grains in Weld Metal of Higher Heat Input.

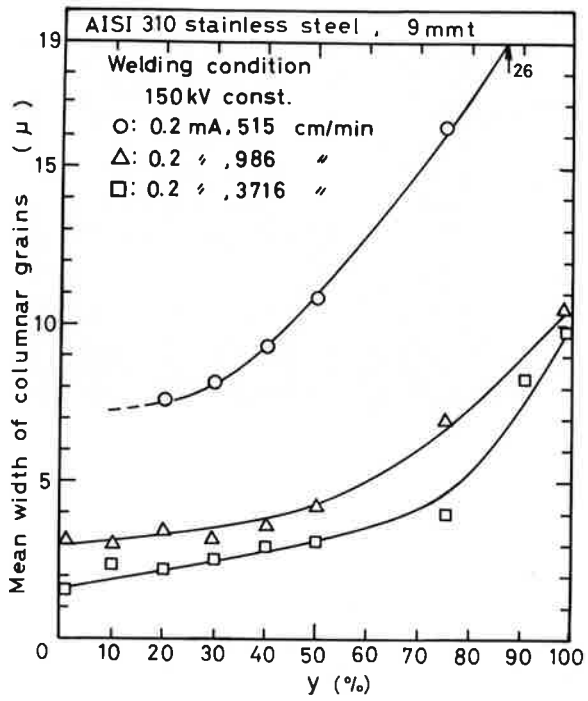

Fig. 4 Variation of Mean Width of Columnar Grains in Weld Metal of Lower Heat Input.

The variations in the columnar crystal grain size inward weld metal are shown for electron beam weld metal of AISI 310 stainless steel in Fig. 3 and 4 for higher and lower weld heat input, respectively.

Y in percent in the axis of abscissa represents the location in the weld metal which indicates the fusion boundary and the center of weld metal for 0 (%) and 100 (%), respectively. In the case of higher weld heat input the mean width increases abruptly with an increase of y (%), however, as the weld heat input decreases, the mean width increases gradually at the high value of y. In the case of lower weld heat input as shown in Fig. 4, an increase in the width is also observed. That is to say, the prefered growth inward weld metal occurs even in case of the weld metal of the lowest weld heat input in this experiment. Generally the smaller the grain size in the fusion boundary, the smaller that in the weld center.

3.2 Size and Feature of Subgrains

(1) Primary Arm Spacing

The variations in the primary arm spacing inward

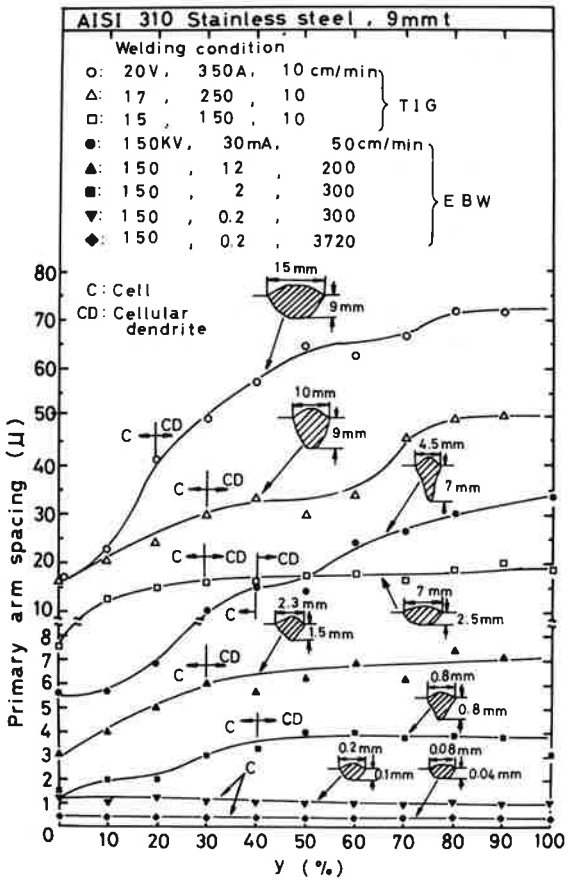

Fig. 5 Variation of Primary Arm Spacing with y (%) in Weld Metal for AISI 310 Stainless Steel.

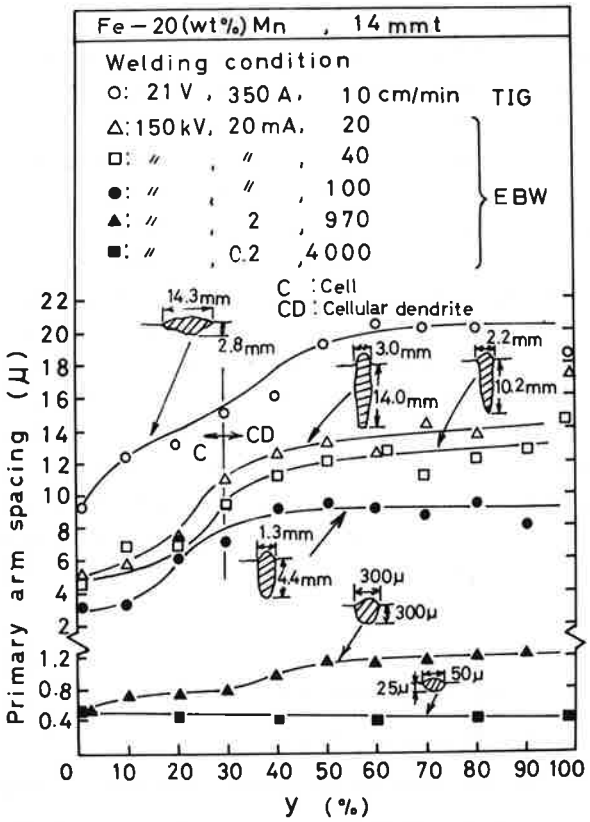

Fig. 6 Variation of Primary Arm Spacing with y (%) in Weld Metal for Fe-20 (wt.%) Mn alloy.

weld metals of AISI 310 stainless steel and Fe-20% Mn alloy which were welded with various weld heat input of TIG arc and electron beam are shown in Fig. 5 and 6, respectively.

In the weld metal with higher weld heat input of TIG arc, the primary arm spacings in both weld metals show a considerable increase at 20 to 40 (%) in y and almost constant value thereafter. However in case of the lowest weld heat input the structure of the weld metal shows only cell mode and is not varied in size even in the center of weld metal. The typical structures in the weld metal of AISI 310 stainless steel are compared in Fig. 7(a) and (b) for higher and lower weld heat input, respectively.

The variation of the solidification feature inward weld metal is well explained by the theory of the constitutional supercooling[7–8]. As inward growth proceeds, the growing crystals in the weld metal solidify in the condition of lower temperature gradient and higher solidification rate, that is, a large amount of constitutional supercooling. Therefore the growing mode of the subgrains is gradually varied from cell in the fusion boundary to cellular or columnar dendrite in the weld center, which results in an increase of the primary

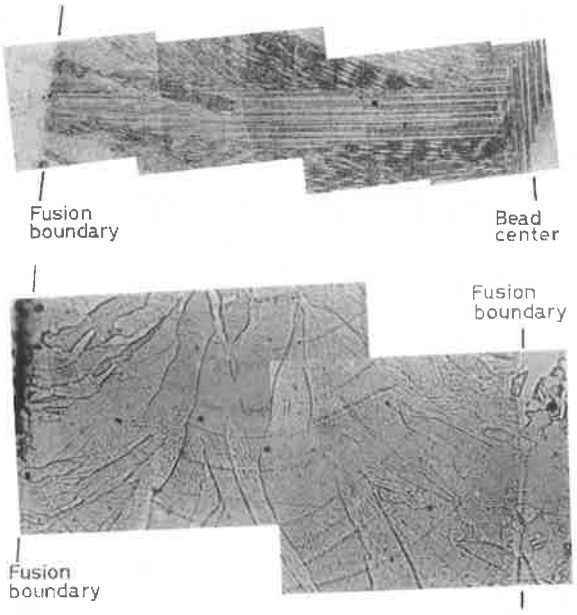

Fig. 7 Structural Changes in Weld Metal of AISI 310 Stainless Steel.
(a) TIG Arc Weld, 17V-250A-10cm/min (x42).
(b) EBW Weld, 150kV-0.2mA-300cm/min (x600).

arm spacing. However in case of the low weld heat input, the cooling rate of the weld metal is extremely increased and the constitutional supercooling is also depressed even in the center of weld metal. Then the structure in this case shows a cell mode in the center of the weld metal and is not varied in size.

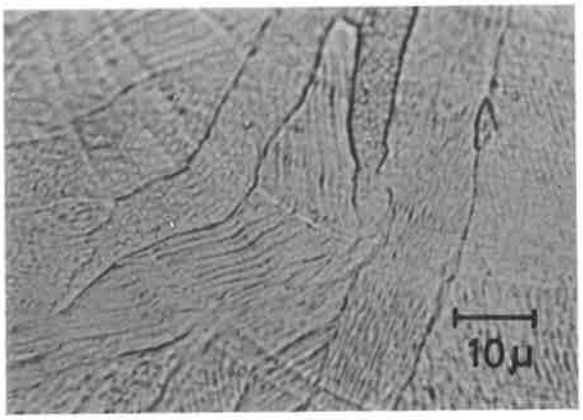

Fig. 8 A Typical Example of Unusual Growth Mode in Cell Structure Observed in Rapidly Solidified Weld Metal.

An interesting feature was often observed in the cell structure of the extreme rapid cooling which is shown in Fig. 8 as an example. The growing direction of the cells is abruptly crooked on the weld ripple line. This is considered that, because of the considerable discrepancy between the growing direction of cell structure and the

direction of heat flow as inward growth proceeds, the different new <100> direction of the crystal start to grow suddenly on the weld ripple line as a substitute for the old <100> direction, which is often observed in the cellular dendritic growth mode in the weld metal of higher weld heat input as indicated in nickel by Savage et al[9].

This sudden change in the growth direction in the cell structure is one of the obvious features in the extreme rapid solidification of weld metal in this investigation.

(2) Secondary Arm Spacing

The variation of the secondary arm spacing in the cellular dendritic solidification structure of the weld metals of AISI 310 stainless steel and Fe-20% Mn alloy which were welded with various weld heat inputs is shown with the location of y in Fig. 9 and 10, respectively. For each weld heat input the secondary arm spacing is considered as a constant for y within a limit of some scattering band. Moreover the secondary arm spacing decreases with a decrease of weld heat input and finally disappears as the cellular dendritic mode is changed to the cell mode in case of the extreme low weld heat input as mentioned before.

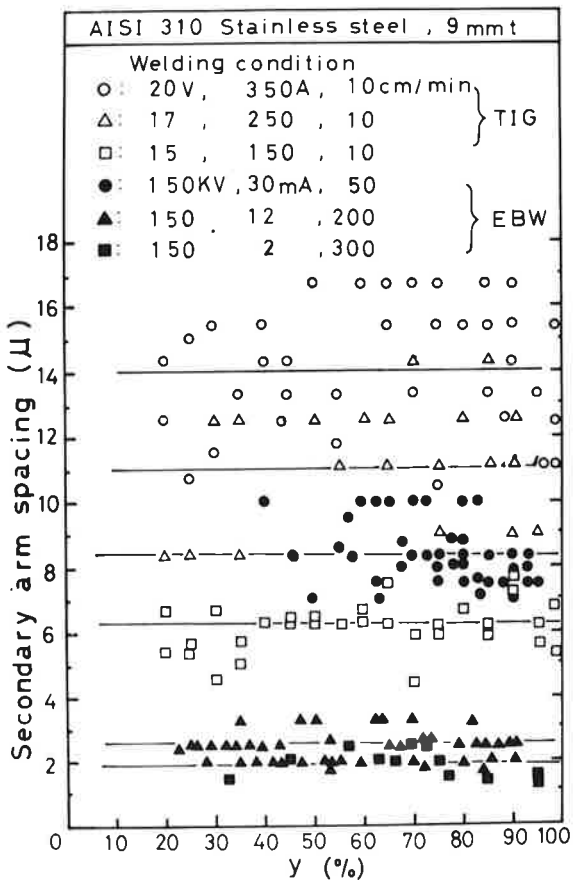

Fig. 9 Variation of Secondary Arm Spacing with y (%) for AISI 310 Stainless Steel.

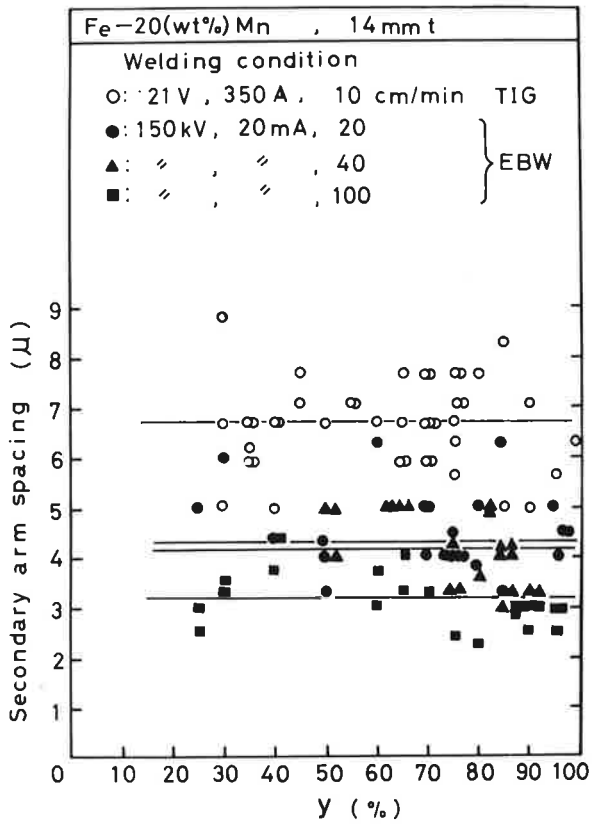

Fig. 10 Variation of Secondary Arm Spacing with y (%) for Fe-20 (wt.%) Mn alloy.

3.3 Relation between Primary and Secondary Arm Spacings and Solidification Rate

As mentioned in the above, the size in the substructures decreases with an increase of solidification rate. Now the relations between the solidification rate and the primary and the secondary arm spacings in the structure of the weld metals are shown in Fig. 11 and 12 for AISI 310 stainless steel and Fe-20% Mn alloy, respectively. It seems that the primary arm spacing is in inverse proportion to 0.45 power for AISI 310 and to 0.4 power for Fe-20% Mn alloy for solidification rate. If

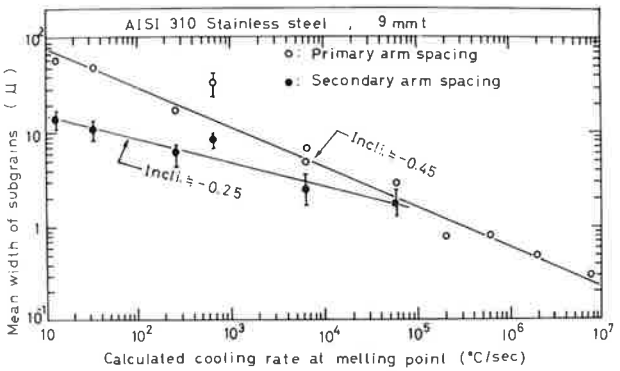

Fig. 11 Relation between Calculated Cooling Rate and Mean Width of Subgrains for AISI 310 Stianless Steel.

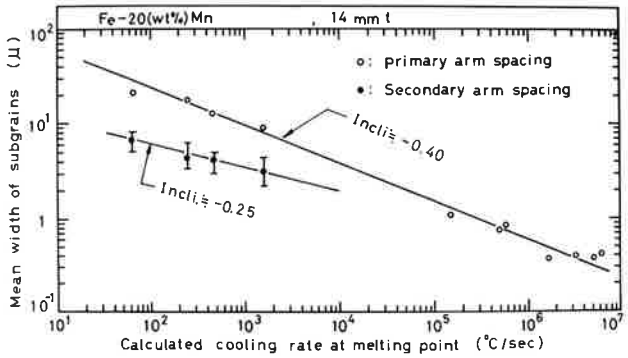

Fig. 12 Relation between Calculated Cooling Rate and Mean Width of Subgrains for Fe-20 (wt.%) Mn alloy.

the primary arm spacing is depended on the diffusion distance of the solute during solidification, then it will be in inverse proportion to 0.5 power for solidification rate. From the experimental results of 0.45 and 0.4 the diffusion of the solute would govern the size of the primary arm spacing although the values are smaller than 0.5. The relation of this kinds has been reported in the solidification of casting[10].

For the secondary arm spacing it is considered in inverse proportion to 0.25 power for solidification rate for both metals of AISI 310 and Fe-20% Mn alloy judging from the results of Fig. 11 and 12.

This value can not be explained by the diffusion phenomena as the primary arm spacing. For slow cooling casting it is said[10] that the secondary arm spacing is in inverse proportion to 1/3 to 1/4 power for solidification rate. Therefore, there is a good agreement in principle between the slow cool casting and the rapid cool welding. This explains that the solidification phenomena in the rapid cooling as welding is similar to that the slow cooling as casting.

4. Conclusions

(1) As inward growth proceeds in the weld metal, the coarsening of the columnar crystal grains occurred even if the weld heat input is so reduced and the solidification cooling rate is raised to about 10^6 °C/sec or more. The prefered growth of the grains could not be obstructed by the rapid solidification in the weld metal within the authors' experiment.

(2) The solidification mode in the substructure of the weld metals was cellular dendrite in the ranges of the low solidification rate less than about 10^5 °C/sec for AISI 310 stainless steel and less than 10^3 °C/sec for Fe-20% Mn alloy and was cell structure with or without cellular dendrite over than these cooling rates. In the extreme rapid cooling of about 10^6 °C/sec the solidification mode was completely cell structure.

(3) In the cellular dendritic structure the primary arm spacing is raised considerably at 20 to 40 % in y which shows the location inward weld metal and gradually thereafter. However the secondary arm spacing was not changed with the variation of y but was depended on the weld heat input related to solidification rate.

(4) The primary and the secondary arm spacings in the substructure of the weld metals of AISI 310 stainless steel and Fe-20% Mn alloy are reduced with an increase of the solidification rate.
The primary arm spacing was proportional to about –0.4 to –0.45 power and the secondary arm spacing was also proportional to about –0.25 power to the cooling rate along the centerline of the weld metal.

(5) The size in width of the substructure became slender by 0.3 to 0.5μm at the solidification rate of about 10^6 to 10^7 °C/sec. This substructure did not disappear even in the highest cooling rate within the range of this experiment.

References

1) P. E. Brown and C. M. Adams: Weld. J., 39 (1960) 520S
2) C. M. Adams: Weld. J., 37 (1958) 210S
3) AWS Welding Handbook Fifth Edition (1962), section 15～20
4) K. Isojima and S. Iida: "Studies on Solidification Condition of Weld Meal" (in Japanese)
5) J. N. Lanzafame et al: Weld. J., 52 (1973), 226
6) M. S. Tuker et al: Weld. J., 47 (1968), 82S
7) W. F. Savage, C. D. Lundin and A. H. Aronson: Weld. J., 44 (1965), 175S
8) F. Matsuda, T. Hashimoto and T. Senda: Trans. NRIM, 11 (1969), 43
9) W. F. Savage, C. D. Lundin and T. F. Chase: Weld. J., 47 (1968), 522S
10) For example; T. Okamoto: Tetsu to Hagane, 58 (1972), 112 (in Japanese)